OL Organic Letters

Letter

pubs.acs.org/OrgLett

Negative Solvatochromism in a Nitrogen-Linked *p*-Pyridiniumcalix[4]arene Derivative

Veronica Iuliano,[†] Carmen Talotta,[†] Carmine Gaeta,[†] Annunziata Soriente,[†] Margherita De Rosa,[†] Silvano Geremia,[‡] Neal Hickey,[‡] Benedetta Mennucci,[§] and Placido Neri*[,†]

[†]Dipartimento di Chimica e Biologia "A. Zambelli", Università di Salerno, Via Giovanni Paolo II 132, I-84084 Fisciano, Salerno, Italy

[‡]Centro di Eccellenza in Biocristallografia, Dipartimento di Scienze Chimiche e Farmaceutiche, Università di Trieste, via L. Giorgieri 1, I-34127 Trieste, Italy

[§]Dipartimento di Chimica Industriale, Università di Pisa, Via G. Moruzzi 13, I-56124 Pisa, Italy

Supporting Information

ABSTRACT: In this paper, we report the synthesis, structural characterization, and solvatochromic properties of a nitrogen-linked *p*-pyridiniumcalix[4]arenediol derivative **1**. In the solid state, **1** forms a dimeric capsule stabilized by a network of weak H-bonding interactions involving acetonitrile solvent molecules. In solution, **1** shows a peculiar negative solvatochromism which was rationalized with the aid of TD-DFT calculations. The specie responsible for this phenomenon is the monodeprotonated betainic form of **1** which is easily formed at pH close to neutrality.

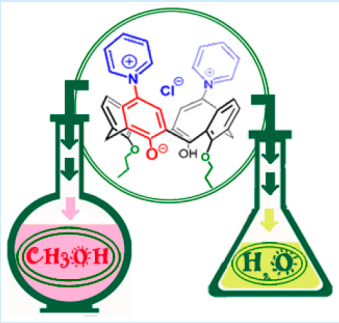

Solvatochromism is a phenomenon in which one observes a change in absorption and/or emission spectra of a chromophore by changing the solvent polarity.[1] It is a complex phenomenon in which the secondary interactions between solvent and chromophore play a crucial role. This complexity has important direct consequences in the wide use that solvatochromism has in many fields ranging from chemical to biological applications.[2] It is commonly used to study local and mass polarity in macrosystems[3] or even the conformation and binding of proteins.[4] Furthermore, solvatochromism plays a key role in the study of dyes, especially those of cyanine[5] and merocyanine.[6] Among the chromophores investigated, the pyridinium-*N*-phenolate dyes constitute a benchmark thanks to their unique solvatochromic properties.[7] On the other hand, calix[*n*]arenes[8] are versatile compounds widely recognized for their role in host−guest chemistry.[9] In the last decades, many efforts have been devoted to designing chromogenic calix[*n*]-arene derivatives.[10] Chromogenic calixarene hosts are able to change their absorption or fluorescence spectra in the presence of metal cation guests.[11] On this basis, Bitter[10] and co-workers reported chromoionophore calixarene derivatives bearing a pyridinium moiety in conjugation with a dissociable calixarene−phenolic group. These chromogenic calixarene derivatives were able to perform the quantitative determination of the physiologically essential cations Na^+, Li^+, and Ca^{2+}.[10]

The Zincke reaction is a useful tool to introduce a pyridinium moiety on active positions of aromatic rings.[12] Previously, Bucher[13] and co-workers exploited the Zincke reaction in order to functionalize the upper rim of calixarene macrocycle with 4,4′-bipyridinium moieties. Prompted by these considerations, we planned to synthesize the *p*-pyridiniumcalix[4]arene derivative **1** (Scheme 1) and to explore its solvatochromic properties with the aid of quantum chemical calculations. In addition, the solid-state self-assembly properties of its hexafluorophosphate salt $\mathbf{1}\cdot(PF_6^-)_2$ were also investigated by X-ray diffraction. Derivative $\mathbf{1}\cdot(Cl^-)_2$ was synthesized by coupling the known diamino derivative **2**[14] with the Zincke salt **3**[15] (Scheme 1). The reaction was carried out in a mixture of ethanol/water (4:1, v/v) under MW irradiation to give $\mathbf{1}\cdot(Cl^-)_2$ in 46% yield. The salt $\mathbf{1}\cdot(Cl^-)_2$ was completely characterized by 1D (SI) and 2D NMR studies (SI). These studies confirmed that $\mathbf{1}\cdot(Cl^-)_2$ adopts in solution a cone conformation as evidenced by the presence of an AX system

Scheme 1. Synthesis of *p*-Pyridiniumcalix[4]arene $\mathbf{1}\cdot(X^-)_2$

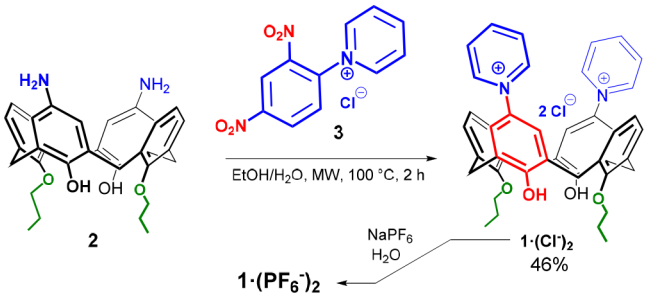

Received: February 22, 2019

attributable to the $ArCH_2Ar$ groups at 4.41 and 3.54 ppm in its ^1H NMR spectrum (CD_3OD, 600 MHz, 298 K). Regarding the *p*-pyridinium group, three signals were found at low fields between 9.20 and 8.20 ppm. At this point, we attempted to grow crystals of $\mathbf{1}\cdot(Cl^-)_2$ suitable for X-ray crystallography in order to confirm its structure and to study its solid-state self-assembly properties. However, no suitable crystals were obtained under the different conditions explored by us. Thus, we decided to exchange the chloride with the hexafluorophosphate as the counteranion (Scheme 1).

The salt $\mathbf{1}\cdot(PF_6^-)_2$ was completely characterized by 1D (SI) and 2D NMR studies (SI). Crystals suitable for X-ray diffraction analysis were obtained by slow evaporation of an acetonitrile/water solution. The asymmetric unit of the centrosymmetric triclinic crystal contains one $\mathbf{1}\cdot(PF_6^-)_2$ unit and three acetonitrile solvent molecules. The calixarene macrocycle of $\mathbf{1}\cdot(PF_6^-)_2$ adopts a cone conformation stabilized by two intramolecular O−H···O H-bonds on the lower rim (O···O distances: 2.70 and 2.72 Å) (Figure 1a). One acetonitrile solvent molecule is hosted deep within the aromatic cavity of the calixarene macrocycle (ACN molecule with yellow C atoms, Figure 1a). This is stabilized by C−H···π interactions between its methyl group and the propoxy-substituted aromatic rings as well as a weak H-bond interaction[16] between its nitrogen atom and the α-H atom of a pyridinium group. Interestingly, the fact that this ACN molecule acts both as a H-bond donor and acceptor implies that these interactions synergically reinforce each other. The crystal packing shows that two macrocycles of **1**, related by a symmetry inversion center, face each other to form a supramolecular pocket (Figure 1b). The closest contacts between the two calixarenes involves only the pyridinium arms, which results in a rather open structure. The alignment of the dimeric supramolecular pockets along the *a*-axis creates parallel open channels in the crystal (Figure 1c). These channels are filled by ACN solvent molecules. In addition to the ACN molecule hosted deep within the calixarene cavities, the other two solvent molecules lie in the open channels. One lies inside the pocket (ACN molecules with green C atoms, Figure 1b) oriented in an antiparallel fashion with respect to the molecule hosted in the cavity, while the second is located between adjacent pockets (ACN molecules with magenta C atoms, Figure 1d). The PF_6^- anions play a key role in the formation of the crystal structure, as they are located along the *a*-axis, sandwiched between the pyridinium arms of adjacent calixarenes and counterbalancing the positive charge. All fluorine atoms are also involved in various weak H-bond interactions with aromatic hydrogen atoms of the calixarenes, as well as with solvent molecules. A description of the overall H-bond network is given in the Supporting Information. Concerning the solvatochromic properties of $\mathbf{1}\cdot(Cl^-)_2$, in Figure 2 we report its UV−vis spectra in two representative polar solvents: water and methanol. When the *p*-pyridiniumcalix[4]arene derivative was dissolved in water, the solution was yellow, while in methanol its solution turned pink.

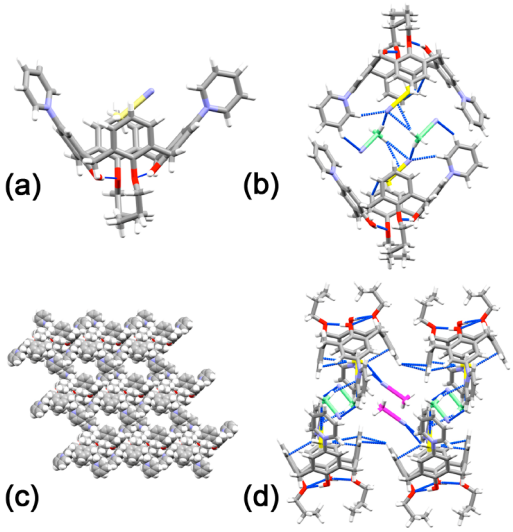

Figure 1. Representation of the solid-state structure of $\mathbf{1}\cdot(PF_6^-)_2$. (a) $CH_3CN \subset \mathbf{1}$ host−guest complex showing a deeply hosted acetonitrile molecule (yellow C atoms). (b) Centrosymmetric dimeric pocket ($\mathbf{1}_2$) containing two pairs of symmetry independent acetonitrile molecules (yellow and green C atoms). (c) Space-filling representation of the open channels formed by dimeric supramolecular pocket alignment along the *a*-axis. (d) Third symmetry-independent acetonitrile molecules in the channels between the pockets (magenta C atoms), as viewed orthogonally to the *a*-axis.

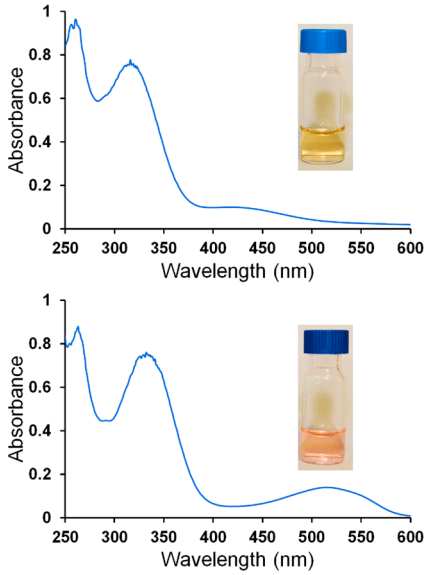

Figure 2. (Top) UV−vis spectrum of derivative $\mathbf{1}\cdot(Cl^-)_2$ in water. (Bottom) UV−vis spectrum of derivative $\mathbf{1}\cdot(Cl^-)_2$ in methanol.

The UV−vis spectrum of $\mathbf{1}\cdot(Cl^-)_2$ in water shows three different bands at λ = 260, 316, and 420 nm (Figure 2). Interestingly, when the solvent was changed to methanol, the band at 420 nm undergoes a significant red-shift at 515 nm (Figure 2), while the other two are shifted at 263 and 330 nm. In summary, $\mathbf{1}\cdot(Cl^-)_2$ undergoes a significant blue-shift as the polarity of the solvent increases in accord with a negative solvatochromism. The experimental investigation has been accompanied to and integrated with quantum chemical calculations using density functional theory (DFT), and its time-dependent (TD-DFT) extension, in combination with the polarizable continuum model (PCM)[17] to include the effects of the different solvents. The D3 correction proposed by Grimme[18] has been also included to account for dispersion effects. All calculations have been performed using the B3lyp functional in combination with the 6-31G(d) basis set for the geometry optimizations and the 6-31+G(d) for the electronic excitations. The excitation energies have been finally corrected

DOI: 10.1021/acs.orglett.9b00683
Org. Lett. XXXX, XXX, XXX−XXX

for the effects of the relaxation of the solvent polarization through the corrected Linear Response model.[19] The G09 software has been used for all of the calculations.[20]

At first, the geometry of the *p*-pyridiniumcalix[4]arene derivative **1** was optimized in methanol and in water. In the case of methanol, we have also investigated the possible effect of the counterion (Cl^-). In water, instead, we have included two explicit solvent molecules H-bonded to the hydroxyl groups. All of the optimized structures present the same cone conformation in agreement with the crystallographic data (Figure S19). The presence of the counteranion induces only a small decrease in the aperture of the cone, while when moving from methanol to water we do not observe any significant change until we add the two H-bonded waters which lead to a more open cone (the distance, *d*, between the two carbon atoms linked to the pyridinium groups changes from 8.5 to 9.7 Å, Figure S19). The optimized structures have been finally used to compute vertical excitation energies. In both solvents, the resulting picture is conserved with the presence of two almost degenerate excitations in the region 300−500 nm. They are found at ca. 309 nm in methanol and 303 nm in water (the third, much less intense, excitation is found at about 240 nm in both solvents). These results seem to indicate that the solvatochromic band measured at 515 nm in methanol and 420 nm in water cannot be explained in terms of a single protonation state but that possible deprotonated structures have to be present. To confirm this hypothesis, we have repeated the geometry optimization and the calculation of the excitation energies for the mono- and the bis-deprotonated structures in methanol. The deprotonation induces a significant closure of the cone where the *d* distance reduces to 6.9 and 4.6 Å in the mono- and bis-deprotonated structures, respectively (Figure S19). When the monodeprotonated structure is finally used to simulate the absorption spectrum, we observe a red-shift of the previously found band from 309 to 320 nm. However, the most striking difference is the appearance of a new low-energy excitation at 490 nm. These two features lead the whole picture in much better agreement with the measured spectra. When we consider the bis-deprotonated structure, only one band survives in the region 300−600 nm and it is found at 482 nm; this finding seems to suggest that this protonation state is not relevant under the present conditions. In order to evaluate the solvatochromism, the monodeprotonated system has been also investigated in water. In the latter case, we have also included one explicit water molecule hydrogen-bonded to the negatively charged oxygen. The obtained results show that the low-energy excitation ($S_1 \leftarrow S_0$) moves from 481 to 463 nm when we include the H-bonded water molecule; the latter, in fact, stabilizes the HOMO orbital, thus explaining the observed blue-shift (Figure 3). If now we compare this value with the one obtained in methanol, we observe that this band is characterized by a negative solvatochromism in agreement with experiments. This effect is mainly due to the larger stabilization of the HOMO orbital by hydrogen bonding (Figure 3).

Interestingly, the monomeric 4-pyridiniumphenoxide (4-PPO) shows the solvatochromic longest band at 365 and 394 nm in H_2O and MeOH, respectively,[21] values significantly lower than that observed when the 4-PPO moiety is embedded in the macrocyclic structure of **1** (420 and 515 nm, respectively). In order to confirm the presence of deprotonated forms under the experimental conditions, we decided to study the absorption properties of **1**·$(Cl^-)_2$ at different pH. In Figure 4 we report the UV−vis titration of **1**·$(Cl^-)_2$ with $(n\text{-Bu})_4$NOH in methanol.[22] Initially, the absorption spectrum of **1**·$(Cl^-)_2$ in acidified methanol (1 μL of 1 N aqueous solution of HCl) shows a band at 334 nm, which disappears upon addition of base. At once two new bands appear in the UV−vis spectrum of **1**·$(Cl^-)_2$ after addition of base, at 307 and 473 nm with an isosbestic point at 310 nm. The pK_{a1} value of **1**·$(Cl^-)_2$ was also determined by potentiometric titration using a pH electrode and titrating the *p*-pyridiniumcalix[4]arene **1**·$(Cl^-)_2$ with $(n\text{-Bu})_4$NOH. By interpolation data, a dissociation constant value of $K_{a1} = 1.99 \times 10^{-5}$, $pK_{a1} = 4.7$ was found. This datum provides an experimental support to the above hypothesis of the presence of deprotonated forms. In fact, on this basis, the mono-deprotonated system, which theoretically was found responsible of the observed negative solvatochromism, is the most abundant form at the neutral experimental pH.

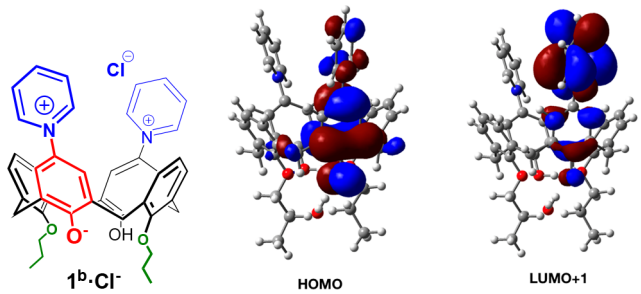

Figure 3. Molecular orbitals involved in the lowest excitation for the monodeprotonated betainic form $\mathbf{1}^b$ when H-bonded to a water molecule.

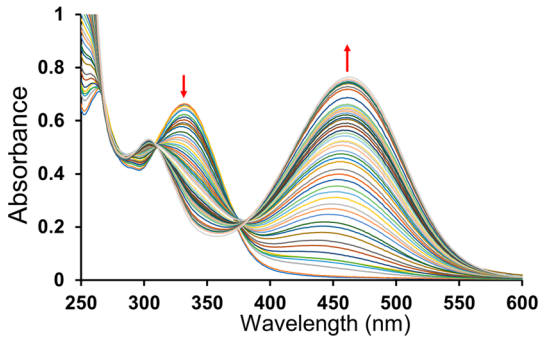

Figure 4. UV−vis titration of *p*-pyridiniumcalix[4]arene **1**·$(Cl^-)_2$ with $(n\text{-Bu})_4$NOH (from 0 to 70 equiv) in methanol.

In conclusion, we have here reported a new calix[4]-arenediol derivative **1** bearing two conjugated pyridinium moieties *N*-linked at its phenolic para positions. In the solid state, **1** forms a dimeric capsule stabilized by a network of weak H-bonding interactions involving CH_3CN solvent molecules. In solution, *p*-pyridiniumcalix[4]arene **1** shows an interesting negative solvatochromism which was rationalized with the aid of TD-DFT quantum chemical calculations. It was found that the species responsible for this phenomenon is the monodeprotonated betainic form, which is very abundant at the experimental neutral pH. We are convinced that further examples of solvatochromic calixarene derivatives will provide interesting potential applications in chemistry and biology.

DOI: 10.1021/acs.orglett.9b00683
Org. Lett. XXXX, XXX, XXX−XXX

■ ASSOCIATED CONTENT

Supporting Information

The Supporting Information is available free of charge on the ACS Publications website at DOI: 10.1021/acs.orglett.9b00683.

Details of experimental procedures, 1D and 2D NMR spectra, fluorescence spectra, UV−vis titration, determination of the p*K*a of **1**·$(Cl^-)_2$, TDDFT results, and Cartesian coordinates of the DFT-optimized structures (PDF)

Accession Codes

CCDC 1892913 contains the supplementary crystallographic data for this paper. These data can be obtained free of charge via www.ccdc.cam.ac.uk/data_request/cif, or by emailing data_request@ccdc.cam.ac.uk, or by contacting The Cambridge Crystallographic Data Centre, 12 Union Road, Cambridge CB2 1EZ, UK; fax: +44 1223 336033.

■ AUTHOR INFORMATION

Corresponding Author

*E-mail: neri@unisa.it.

ORCID

Carmen Talotta: 0000-0002-2142-6305
Carmine Gaeta: 0000-0002-2160-8977
Annunziata Soriente: 0000-0001-6937-8405
Margherita De Rosa: 0000-0001-7451-5523
Benedetta Mennucci: 0000-0002-4394-0129
Placido Neri: 0000-0003-4319-1727

Notes

The authors declare no competing financial interest.

■ REFERENCES

(1) (a) Marini, A.; Munoz-Losa, A.; Biancardi, A.; Mennucci, B. *J. Phys. Chem. B* **2010**, *114*, 17128−17135. (b) Reichardt, C. *Solvent and Solvent Effects in Organic Chemistry*, 3rd ed.; Wiley-VCH: Weinheim, 2002. (c) Suppan, P.; Ghoneim, N. *Solvatochromism*; The Royal Society of Chemistry: Cambridge, 1997.

(2) Klymchenko, A. S. *Acc. Chem. Res.* **2017**, *50*, 366−375.

(3) Kreder, R.; Pyrshev, K. A.; Darwich, Z.; Kucherak, O. A.; Mely, Y.; Klymchenko, A. S. *ACS Chem. Biol.* **2015**, *10*, 1435−1442.

(4) Klymchenko, A. S. *Acta Chim.* **2012**, *359*, 20−26.

(5) Capobianco, A.; Borrelli, R.; Landi, A.; Velardo, A.; Peluso, A. *J. Phys. Chem. A* **2016**, *120*, 5581−5589.

(6) (a) Kulinich, A. V.; Mikitenko, E. K.; Ishchenko, A. A. *Phys. Chem. Chem. Phys.* **2016**, *18*, 3444−3453. (b) Kulinich, A. V.; Ishchenko, A. A.; Bulavko, G. V.; Davidenko, N. A. *Theor. Exp. Chem.* **2018**, *54*, 178−185.

(7) (a) Reichardt, C. *Pure Appl. Chem.* **2008**, *80*, 1415−1432. (b) Machado, V. G.; Stock, R. I.; Reichardt, C. *Chem. Rev.* **2014**, *114*, 10429−10475. (c) Cha, S.; Choi, M. G.; Jeon, H. R.; Chang, S.-K. *Sens. Actuators, B* **2011**, *157*, 14−18. (d) Jacques, P.; Graff, B.; Diemer, V.; Ay, E.; Chaumeil, H.; Carré, C.; Malval, J. P. *Chem. Phys. Lett.* **2012**, *531*, 242−246.

(8) (a) Gutsche, D. *Calixarenes: An introduction, The Royal Society of Chemistry*: Cambridge, 2008. (b) *Calixarenes and Beyond*; Neri, P., Sessler, J. L., Wang, M.-X., Eds.; Springer: Dordrecht, The Netherlands, 2016.

(9) (a) Gaeta, C.; Talotta, C.; Farina, F.; Teixeira, F. A.; Marcos, P. M.; Ascenso, J. R.; Neri, P. *J. Org. Chem.* **2012**, *77*, 10285−10293. (b) Gaeta, C.; Talotta, C.; Margarucci, L.; Casapullo, A.; Neri, P. *J. Org. Chem.* **2013**, *78*, 7627−7638. (c) Talotta, C.; Gaeta, C.; De Rosa, M.; Ascenso, J. R.; Marcos, P. M.; Neri, P. *Eur. J. Org. Chem.* **2016**, *2016*, 158−167.

(10) (a) Bitter, I.; Grün, A.; Tóth, G.; Szöllósy, Á.; Horváth, G.; Ágai, B.; Tőke, L. *Tetrahedron* **1996**, *52*, 639−646. (b) Bitter, I.; Grün, A.; Tőke, L.; Tóth, f.; Balázs, B.; Mohammed-Ziegler, I.; Grofcsik, A.; Kubinyi, M. *Tetrahedron* **1997**, *53*, 16867−16876.

(11) Ikeda, A.; Shinkai, S. *Chem. Rev.* **1997**, *97*, 1713−1734.

(12) (a) Wang, Z. *Comprehensive Organic Name Reactions and Reagents*; John Wiley & Sons 2010. (b) Das, G.; Skorjanc, T.; Sharma, S. K.; Gandara, F.; Lusi, M.; Rao, D. S. S.; Vimala, S.; Prasad, S. K.; Raya, J.; Han, D. S.; Jagannathan, R.; Olsen, J. C.; Trabolsi, A. *J. Am. Chem. Soc.* **2017**, *139*, 9558−9565.

(13) Kahlfuss, C.; Milet, A.; Wytko, J.; Weiss, J.; Saint-Aman, E.; Bucher, C. *Org. Lett.* **2015**, *17*, 4058−4061.

(14) Struck, O.; Chrisstoffels, L. A. J.; Lugtenberg, R. J. W.; Verboom, W.; van Hummel, G. J.; Harkema, S.; Reinhoudt, D. N. *J. Org. Chem.* **1997**, *62*, 2487−2493.

(15) Robertson, L.; Hartley, R. C. *Tetrahedron* **2009**, *65*, 5284−5292.

(16) Steiner, T. *Angew. Chem., Int. Ed.* **2002**, *41*, 48−76.

(17) Mennucci, B. *WIREs Comput. Mol. Sci.* **2012**, *2*, 386−404.

(18) Grimme, S. *WIREs Comput. Mol. Sci.* **2011**, *1*, 211−228.

(19) Caricato, M.; Mennucci, B.; Tomasi, J.; Ingrosso, F.; Cammi, R.; Corni, S.; Scalmani, G. *J. Chem. Phys.* **2006**, *124*, 124520−13.

(20) Frisch, M. J. et al. *Gaussian 09*, revision A.02; Gaussian, Inc.: Wallingford, CT, 2016. See the SI for the full reference.

(21) González, D.; Neilands, O.; Caroli Rezende, M. *J. Chem. Soc., Perkin Trans. 2* **1999**, 713−717.

(22) (a) Diemer, V.; Chaumeil, H.; Defoin, A.; Jacques, P.; Carré, C. *Tetrahedron Lett.* **2005**, *46*, 4737−4740. (b) Reijenga, J.; van Hoof, A.; van Loon, A.; Teunissen, B. *Anal. Chem. Insights* **2013**, *8*, 53−71. (c) Babić, S.; Horvat, A. J. M.; Mutavdžić Pavlović, D.; Kaštelan-Macan, M. *TrAC, Trends Anal. Chem.* **2007**, *26*, 1043−1061.

DOI: 10.1021/acs.orglett.9b00683
Org. Lett. XXXX, XXX, XXX−XXX